

ARMY RESEARCH LABORATORY



## **Mechanical Response and Shear Initiation of Double-Base Propellants**

**by Stephan R. Bilyk and Michael J. Scheidler**

**ARL-RP-260**

**August 2009**

*A reprint from the Proceedings of the 13th International Detonation Symposium,  
Norfolk, VA, 23–28 July 2006.*

## **NOTICES**

### **Disclaimers**

The findings in this report are not to be construed as an official Department of the Army position unless so designated by other authorized documents.

Citation of manufacturer's or trade names does not constitute an official endorsement or approval of the use thereof.

Destroy this report when it is no longer needed. Do not return it to the originator.

# **Army Research Laboratory**

Aberdeen Proving Ground, MD 21005-5066

---

---

**ARL-RP-260**

**August 2009**

---

---

## **Mechanical Response and Shear Initiation of Double-Base Propellants**

**Stephan R. Bilyk and Michael J. Scheidler**  
**Weapons and Materials Research Directorate, ARL**

A reprint from the *Proceedings of the 13th International Detonation Symposium*,  
Norfolk, VA, 23–28 July 2006.

REPORT DOCUMENTATION PAGE			Form Approved OMB No. 0704-0188		
Public reporting burden for this collection of information is estimated to average 1 hour per response, including the time for reviewing instructions, searching existing data sources, gathering and maintaining the data needed, and completing and reviewing the collection information. Send comments regarding this burden estimate or any other aspect of this collection of information, including suggestions for reducing the burden, to Department of Defense, Washington Headquarters Services, Directorate for Information Operations and Reports (0704-0188), 1215 Jefferson Davis Highway, Suite 1204, Arlington, VA 22202-4302. Respondents should be aware that notwithstanding any other provision of law, no person shall be subject to any penalty for failing to comply with a collection of information if it does not display a currently valid OMB control number. <b>PLEASE DO NOT RETURN YOUR FORM TO THE ABOVE ADDRESS.</b>					
1. REPORT DATE (DD-MM-YYYY) August 2009		2. REPORT TYPE Reprint		3. DATES COVERED (From - To) 23-28 July 2000	
4. TITLE AND SUBTITLE Mechanical Response and Shear Initiation of Double-Base Propellants			5a. CONTRACT NUMBER		
			5b. GRANT NUMBER		
			5c. PROGRAM ELEMENT NUMBER		
6. AUTHOR(S) Stephan R. Bilyk and Michael J. Scheidler			5d. PROJECT NUMBER IHEM01-M		
			5e. TASK NUMBER		
			5f. WORK UNIT NUMBER		
7. PERFORMING ORGANIZATION NAME(S) AND ADDRESS(ES) U.S. Army Research Laboratory ATTN: RDRL-WMT-D Aberdeen Proving Ground, MD 21005-5066			8. PERFORMING ORGANIZATION REPORT NUMBER ARL-RP-260		
9. SPONSORING/MONITORING AGENCY NAME(S) AND ADDRESS(ES)			10. SPONSOR/MONITOR'S ACRONYM(S)		
			11. SPONSOR/MONITOR'S REPORT NUMBER(S)		
12. DISTRIBUTION/AVAILABILITY STATEMENT Approved for public release; distribution is unlimited.					
13. SUPPLEMENTARY NOTES A reprint from the <i>Proceedings of the 13th International Detonation Symposium</i> , Norfolk, VA, 23-28 July 2006.					
14. ABSTRACT The intense shearing that occurs in propellants during impulsive loading can lead to initiation. In an effort to determine useful shear initiation criteria, the U.S. Army Research Laboratory has developed a dynamic shear punch test using a modified split-Hopkinson bar. Varying the striker bar's velocity and length controls the shear rate and duration. Shear velocities approaching 100 m/s and durations as long as 0.2 ms are possible. Experimental results have been obtained for several energetic materials and a nonreacting polymer, polycarbonate (PC). This report presents a detailed analysis used to obtain constitutive behavior and shear initiation for double-base propellants and computational results of the shear punch test. For the simulations, the viscoSCRAM constitutive model was used to describe viscoelasticity, cracking and ignition in the propellant when subjected to dynamic shear loading conditions. First, we will present the analysis used to obtain viscoelastic material parameters. The stress relaxation function for the linear viscoelastic response was obtained by using time-temperature superposition to generate a master curve from Dynamic Mechanical Analysis (DMA) data. Next, the effect of initial crack size and critical hot spot duration on the ignition threshold temperature was examined. The validity of the constitutive relation, failure criterion, and shear initiation is determined based on their ability to predict the observed response from the dynamic shear punch test.					
15. SUBJECT TERMS insensitive munitions, double-base propellants, shear initiation, viscoSCRAM, ALE3D					
16. SECURITY CLASSIFICATION OF:			17. LIMITATION OF ABSTRACT  UU	18. NUMBER OF PAGES  16	19a. NAME OF RESPONSIBLE PERSON Stephan R. Bilyk
a. REPORT Unclassified	b. ABSTRACT Unclassified	c. THIS PAGE Unclassified			19b. TELEPHONE NUMBER (Include area code) 410-278-2976

# MECHANICAL RESPONSE AND SHEAR INITIATION OF DOUBLE-BASE PROPELLANTS

Stephan R. Bilyk and Michael J. Scheidler

Weapons and Materials Research Directorate  
U.S. Army Research Laboratory  
Aberdeen Proving Ground, MD 21005

**Abstract.** The intense shearing that occurs in propellants during impulsive loading can lead to initiation. In an effort to determine useful shear initiation criteria, the U.S. Army Research Laboratory has developed a dynamic shear punch test using a modified split-Hopkinson bar. Varying the striker bar's velocity and length controls the shear rate and duration. Shear velocities approaching 100 m/s and durations as long as 0.2 ms are possible. Experimental results have been obtained for several energetic materials and a nonreacting polymer, polycarbonate (PC). This paper presents a detailed analysis used to obtain constitutive behavior and shear initiation for double-base propellants and computational results of the shear punch test. For the simulations, the viscoSCRAM constitutive model was used to describe viscoelasticity, cracking and ignition in the propellant when subjected to dynamic shear loading conditions. First, we will present the analysis used to obtain viscoelastic material parameters. The stress relaxation function for the linear viscoelastic response was obtained by using time-temperature superposition to generate a master curve from Dynamic Mechanical Analysis (DMA) data. Next, the effect of initial crack size and critical hot spot duration on the ignition threshold temperature was examined. The validity of the constitutive relation, failure criterion, and shear initiation is determined based on their ability to predict the observed response from the dynamic shear punch test.

## INTRODUCTION

Energetic materials are often ranked in terms of their sensitivity when subjected to shock, shear, and thermal stimuli. The goal for military applications is to develop initiation criteria under each stimuli as well as a fundamental understanding of coupled behavior. Several useful analytical models and experiments already exist for shock and thermal stimuli. However, initiation due to shear loading is complex and poorly understood. Many hazardous scenarios such as hot metal fragments impacting an explosive canister can lead to shear initiation of an energetic. Shear initiation occurs at timescales over

tens or hundreds of microseconds, an order of magnitude larger than shock loading. Energy is deposited in localized regions causing a local temperature rise, which for some energetics can even lead to the development of adiabatic shear bands.

It is generally accepted that initiation of an energetic is a thermal process<sup>1</sup>. High pressure accelerates chemical reactions, but most often does not initiate them. Therefore, critical factors to initiate reaction are those that generate heat by direct application or by the conversion of mechanical or electrical energy to heat. This paper describes *non-shock mechanical stimuli* sufficient

to create local regions, so called “hot spots”, which can lead to thermal ignition. By non-shock ignition we mean that there is an energy release but no shock wave.

For thermal ignition due to mechanical stimulus, it is not necessary to heat the bulk of the energetic since the locally created hot spots may reach sufficiently high temperatures. Energetic materials are a heterogeneous mixture of polycrystalline explosive, binder, and additives including voids created during material processing. Mechanical loading can nucleate hot spots (commonly in void regions) but only a few become critical hot spots. These critical hot spots ignite the energetic if the generation of heat in the localized volume is greater than the heat lost to the surroundings. In their monograph research on the topic, Bowden and Joffe<sup>2</sup> estimated critical hot spot parameters as typically of micron size (0.1-10 $\mu$ m), lasting for 10 $\mu$ s to 1ms, and reaching temperatures of approximately 700K. Clearly, if local temperatures are high, the size and duration can be smaller. Hot spots form during the interaction of stress waves with material defects and depend on the mechanical, thermal and chemical properties of the energetic. There are different mechanisms at the microstructural length scale that can create hot spot ignition. These include jetting of material grains, hydrodynamic pore collapse, viscous heating, shear localization, friction between grains, internal shear and shock interaction with second phase particles<sup>3,4</sup>. The dominant mechanism for producing the hot spot has not been generally agreed upon. However, Dienes<sup>5</sup> analytically showed that the largest contribution to potential heat generation is the frictional forces on shear crack surfaces.

Double base propellants are composed of nitrocellulose and stirred with a reactive plasticizer liquid nitrate ester such as nitroglycerine which also affects the oxygen balance. Stabilizers and gelatinizers are often added and the paste is hot rolled processed and pressed without the use of a solvent. The plasticizer is used to adjust the oxygen balance which affects the energy output and reaction temperature<sup>6</sup>. This class of propellant powders is often used in large caliber guns and solid rockets.

Initially, the activator punch test was developed to study shear initiation<sup>7</sup>. This test was limited since it was difficult to control the shear velocity independently of the pressure and the

pressure on the shear surface was not well known. Recently, Krzewinski et al.<sup>8</sup> developed a shear punch test at ARL. The shear punch test uses a modified Kolsky bar technique and obtains data for shear initiation of energetic materials subjected to dynamic loading conditions. In addition, some non-energetic polymer materials such as polycarbonate (PC) have been used as surrogate specimens for comparison purposes.

This paper first establishes the shear punch test, describes the constitutive model used for the propellant and finally provides computational results for the shear punch as validation of the energetic material response model.

## EXPERIMENTAL DESCRIPTION

The apparatus used for the shear punch test developed by Krzewinski et al.<sup>8</sup> was a modified Kolsky bar, as shown in Figure 1. The striker, incident, and output bars were 1.27cm diameter 350-maraging steel. The incident and output bars were 150cm in length, while the striker bar was available in 25, 50, and 55cm lengths. The varying striker lengths gave nominal pulse durations of 100, 200, and 220 $\mu$ s, respectively<sup>8</sup>. The specimen had a diameter of 1.905cm and a length of 1.27cm. As the compression wave travels during the entire test, the striker, input and output bars and the holder remain elastic. The specimen is the only material that undergoes plastic deformation but not at constant strain rate.

The experimental measurements are also shown (boxed) in Figure 1. Impact velocity was measured using three fiber optic wires and an optical detector. Two strain gages were mounted near the center of the input and output bars to measure the incident, reflected, and transmitted strains. Finally, a scanning electron microscope (SEM) was used to measure the punch and dent displacements of the specimen as well as examine any fracture regions.

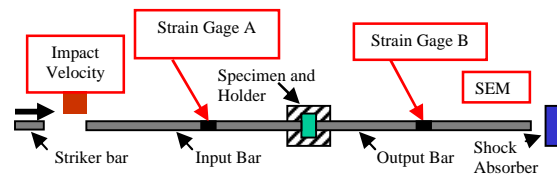


**FIGURE 1. Schematic of Shear Punch Test and data collection (Not to Scale).**

A special shock absorber and transfer piston (not shown in Figure 1) were designed to prevent reverse bar motion whenever the specimen reacted violently. Thin polyethylene disks were also placed between the specimen and incident/output bars for impedance matching. Copper (3mil) and Kaptan (5mil) disks were placed between the striker and incident bar to reduce ringing and wave shape a nearly rectangular incident compressive pulse. The specimen holder was made from 17-4 PH stainless steel and consisted of three pieces held together with six high-strength bolts. In addition, vacuum grease was applied between the specimen and specimen holder to fill any voids and reduce friction at the interfaces. With the applied grease, one can conclude that all initiations occurred because of the shearing within the specimen.

A typical deformed specimen shape observed by Krzewinski et al.<sup>8</sup> is shown in Figure 2. The specimen shown is a double-base propellant, P1. Note also in Figure 2, that the shear surface has localized and runs along the outer radial edges of the incident bar. For this dynamic test, the loading on the P1 specimen was great enough to eventually fracture the specimen along the shear surface.

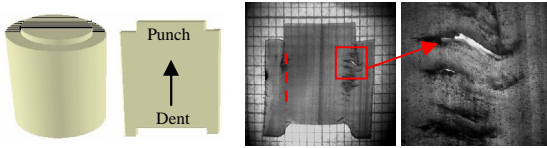


**FIGURE 2. Typical specimen deformation and idealized shear surface (dotted line)<sup>8</sup>.**

## DESCRIPTION OF THE CONSTITUTIVE MODEL

For the simulations, the constitutive behavior of the specimen was modeled using viscoSCRAM<sup>9</sup>. The model captures rate dependence (linear-viscoelastic), damage accumulation (statistical-crack-mechanics), adiabatic mechanical heating and chemical heating that are apparent for some energetics. Furthermore, the model does not include heat conduction because it is too slow compared to the deformation time scale.

The mechanical response has two constitutive assumptions. The first is that the strain rate can be decoupled into viscoelastic and deviatoric material damage components. The second is that the shear stress is determined from

the viscoelastic strain rate. The viscoelastic portion is based on the work of Addessio and Johnson<sup>10</sup> and the damage model uses the statistical crack mechanics (SCRAM) approach of Dienes<sup>11</sup>. The ignition criterion is based on whether the localized temperature increase due to friction between sliding crack faces is sufficient for the hot spot to become critical. The following sub-sections describe each sub-model and relevant material parameters required for each sub-model.

## Viscoelastic Parameters

For sufficiently small strains, the propellant may be modeled as a linear viscoelastic solid. Assuming that the volumetric response is purely elastic, the viscoelastic response is characterized by the stress relaxation function in shear, denoted by  $G$ . This function can be approximated by a sum of decaying exponentials, referred to as a Prony series:

$$G(t) = G_{\infty} + \sum_{n=1}^N G_n e^{-t/\tau_n} \quad (1)$$

Here  $t$  denotes time,  $\tau_n$  are the relaxation times, and  $G_{\infty} = G(\infty)$  is the equilibrium elastic modulus. The coefficients  $G_n$  are also moduli, sometimes referred to as spring constants since this relation may be obtained by analogy with spring and dashpot models. The relation (1) is also known as a generalized Maxwell model. The instantaneous elastic modulus is the value of the stress relaxation function at time zero:

$$G(0) = G_{\infty} + \sum_{n=1}^N G_n \quad (2)$$

It governs the jump in stress across shock waves.

The Prony series approximation to the stress relaxation function is particularly convenient for numerical implementation in explicit codes, as it leads to a simple rate form for the shear stress. For a given material, the number of terms,  $N$ , that is needed in (1) depends on the time window over which the viscoelastic response is to be modeled. For simulations of impact and shock waves, relaxation times on the order of fractions of a nano-second may be needed. On the other hand, relaxation times more than a decade or two larger than the duration of the simulation will yield exponential terms close to unity for all times of interest, so that the corresponding terms in (1) may be lumped into the equilibrium modulus. A general

rule of thumb is that relaxation times should be equally spaced on a log time scale, with at least one term for each decade of time.

The viscoelastic properties of the propellant were obtained by Dynamic Mechanical Analysis (DMA). The response to steady state torsional vibration was measured at six different frequencies from 0.1 Hz to 30 Hz. The shear strains were on the order of 0.1% and thus well within the region of linear viscoelastic response. Each of the fixed frequency tests involved a slow (about 0.5°C/min) temperature sweep from -100°C to 25°C, spanning the glass transition temperature (roughly -58°C). The tests were performed by Rob Jensen of ARL.

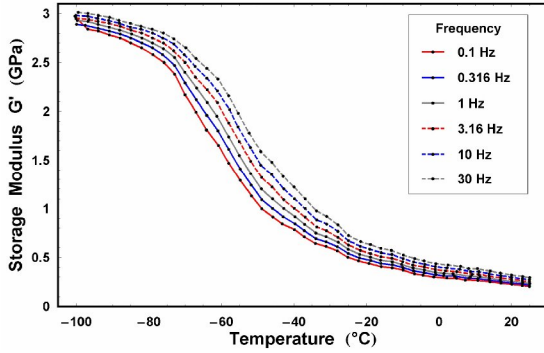


**FIGURE 3. Storage modulus as a function of temperature at six fixed frequencies.**

The storage modulus  $G'$  and loss modulus  $G''$  are obtained from the components of stress in phase with the strain and out of phase with the strain, respectively. They are plotted in Figures 3 and 4. Observe that the peak in the loss modulus is an order of magnitude less than the corresponding value of the storage modulus.

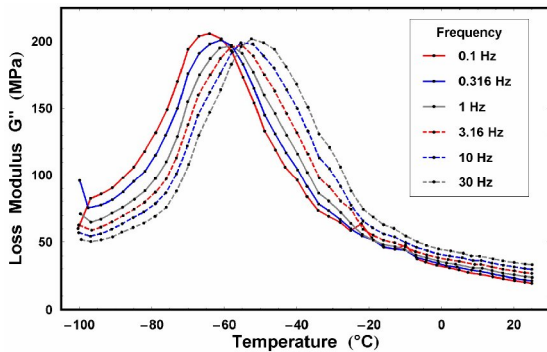


**FIGURE 4. Loss modulus as a function of temperature for six fixed frequencies.**

Another advantage of the Prony series approximation is that it allows, at least in principle, the straightforward determination of the moduli  $G_\infty$  and  $G_n$  in (a) from the DMA data, since in this case the storage modulus  $G'$  is given as a function of the radial frequency  $\omega$  by the relation

$$G'(\omega) = G_\infty + \sum_{n=1}^N G_n \frac{(\tau_n \omega)^2}{1 + (\tau_n \omega)^2} \quad (3)$$

Note that

$$G'(0) = G_\infty \text{ and } G'(\infty) = G(0) \quad (4)$$

Assuming that the number of terms  $N$  and corresponding relaxation times  $\tau_n$  has been chosen, one may determine the values of  $G_\infty$  and  $G_n$  in (3) that best fit the storage modulus data. The difficulty with this approach is that the DMA data does not cover a wide enough frequency range to accurately determine the moduli. This problem is circumvented by using time-temperature superposition (TTS) and involves several steps.

First, the fixed frequency data in Figures 3 and 4 are converted to modulus vs. frequency curves at fixed temperatures. Next, a reference temperature  $T_0$  is selected, and the storage modulus vs. frequency curves at the various temperatures are shifted horizontally relative to the curve corresponding to the reference temperature so as to form a single smooth curve, called a master curve. The principle behind this procedure is the assumption that the temperature dependence of the stress relaxation function  $G$  is governed by the simple relation

$$G(t, T) = G(t/a_T, T_0) \quad (5)$$

where the shift factor  $a_T$  is a decreasing function of the temperature  $T$  with the value 1 at  $T = T_0$ . This implies that all of the relaxation times scale proportionally with temperature:

$$\tau_n(T) = a_T \tau_n(T_0) \quad (6)$$

and that the temperature dependence of the storage and loss moduli are given by

$$G'(\omega, T) = G'(a_T \omega, T_0) ,$$

$$G''(\omega, T) = G''(a_T \omega, T_0) \quad (7)$$

On a log frequency scale, (7) yields the relation

$$G'(\log \omega, T) = G'(\log \omega + \log a_T, T_0) \quad (8)$$

so that modulus vs. log frequency curves at different temperatures superimpose upon shifting horizontally by a temperature-dependent factor. Here,  $T_0$  was chosen to be the glass transition

temperature,  $-58^{\circ}\text{C}$ . The resulting storage modulus master curve is shown in Figure 5. Note that the frequency range has been extended from about  $2\frac{1}{2}$  decades to over 20 decades. The corresponding temperature-dependent horizontal shift factors are given by the upper curve in Figure 6. These “optimal” shift factors were determined so as to yield the smoothest possible curve.

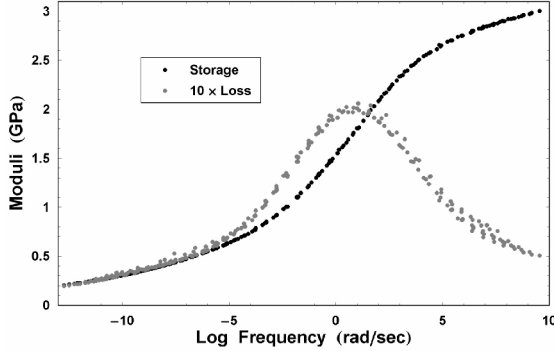


**FIGURE 5. Storage and loss moduli master curves with no vertical shifts, using the optimal horizontal shifts for the storage modulus.**

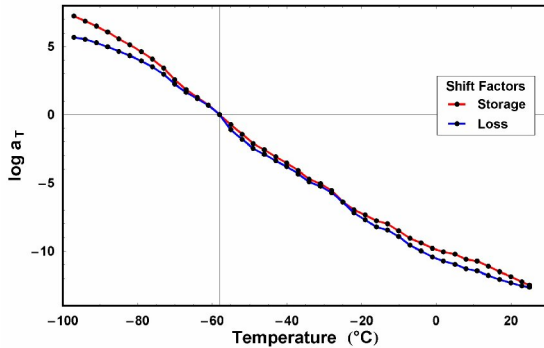


**FIGURE 6. Optimal horizontal shift factors for the storage and loss moduli (no vertical shifts).**

If the principle of TTS were strictly valid, as reflected in the relation (5), then by (7) we see that the same horizontal shift factors should work for both the storage and loss moduli. But in fact the optimal horizontal shift factors for the loss moduli are given by the lower curve in Figure 6. Since the vertical axis is logarithmic, this results in a maximum difference of about  $1\frac{1}{2}$  decades in frequency (equivalently, time) between these shift factors. When the optimal storage modulus shift factors are used to generate the loss modulus master curve, the result is the bell-shaped curve in Figure 5. Note the large scatter, particularly at higher frequencies. Likewise, had the optimal loss

modulus shift factors been used to generate the storage modulus master curve, there would have been a substantial scatter.

A common practice is to overlook these discrepancies and simply fit the coefficients  $G_{\infty}$  and  $G_n$  in (3) to the smooth storage modulus master curve, using the corresponding shift factors for this curve to obtain the temperature dependence of the relaxation times via (6). However, Simon and Ploehn<sup>12</sup> argue against this. In fact, they conclude that “master curves based on superposability of the loss modulus, rather than the storage modulus, may lead to better representations of true response of a material.”

One possible explanation for the discrepancies between the storage and loss modulus shift factors, is temperature dependence of the equilibrium and instantaneous elastic moduli  $G_{\infty} = G(\infty)$  and  $G(0)$ . Observe that (5) implies

$$G(0, T) = G(0, T_0), \quad G(\infty, T) = G(\infty, T_0) \quad (9)$$

That is, the instantaneous and equilibrium elastic moduli are temperature independent. These conclusions are at best approximations. It turns out that even small corrections for the temperature dependence of the instantaneous and equilibrium moduli can lead to substantial changes in the horizontal shift factors.

The correction most commonly used in the polymer literature is

$$G(\infty, T) = \frac{T}{T_0} G(\infty, T_0), \quad (10)$$

where the equilibrium elastic modulus is proportional to the absolute temperature. This relation is supported by experiment as well as the kinetic theory of rubber elasticity. By (4) we see that (10) is equivalent to

$$G'(0, T) = \frac{T}{T_0} G'(0, T_0) \quad (11)$$

Note that the zero here is  $\omega = 0$ , which corresponds to  $\log \omega = -\infty$ . Clearly, when (9) holds, no amount of horizontal shifting can bring the storage modulus vs. frequency curves at different temperatures to coincidence, since they have different low frequency asymptotes. The most common procedure used to correct for this is to first vertically shift the  $G'(\omega, T)$  and  $G''(\omega, T)$  curves by multiplying them by the factor  $T_0/T$ , which in effect cancels out the temperature dependence of the equilibrium modulus. Then the horizontal shifting procedure described above is applied. This

generally works well for temperatures above the glass transition. When applied to the data above, this yielded a slight improvement in the coincidence of the storage and loss shift factors at the higher temperatures, but resulted in substantially worse discrepancies at the lower temperatures. This is due to the fact that the temperature dependence of the instantaneous elastic modulus has not been properly accounted for.

In contrast with the equilibrium modulus, the instantaneous elastic modulus  $G(0, T) = G'(\infty, T)$  should decrease with temperature. McCrum and Pogany<sup>13</sup> and Schapery<sup>14</sup> have emphasized the need to account for this when performing TTS on data below the glass transition temperature. We have essentially followed their procedure here.<sup>a</sup> We omit the details, but the basic idea is as follows. First, the appropriate temperature dependent equilibrium modulus as determined by (10), is subtracted from the storage modulus vs. frequency curve at temperature  $T$ , so that all curves have a low frequency asymptote of zero. However, due to the dependence of  $G'(\infty, T)$  on  $T$ , the high frequency asymptotes of these vertically shifted curves will not coincide, so a second multiplicative scaling is performed to correct for this. We assumed that  $G'(\infty, T)$  varies linearly with  $T$ . Thus the parameters required by this procedure are  $G'(\infty, T_0)$ , the slope  $\beta = dG'(\infty, T)/dT$ , and the value of  $G'(0, T_0)$  for use in (11). Initial estimates for the latter two parameters were obtained from Figure 5. We are not aware of any data from which the slope  $\beta$  could be inferred. The data in Figure 3 provide values for  $dG'(\omega, T)/dT$  only for  $\omega$  in the range from 0.1 to 30 Hz., whereas  $\beta$  is the limit of this derivative as  $\omega \rightarrow \infty$ . We took as our initial estimate for  $\beta$  the smallest slope on the modulus vs. temperature curves in Figure 3. Vertical shifts of the data were performed as described above, followed by horizontal shifts, to obtain a new set of storage and loss modulus master curves.<sup>b</sup> Several iterations were performed, with the three parameters modified slightly at each iteration. The final value of  $\beta$  used was  $-0.004 \text{ GPa}/^\circ\text{C}$ , which is

<sup>a</sup> Their corrections are for the case where the data are compliances, but an analogous procedure works for the moduli.

<sup>b</sup> A slightly different (in fact, simpler) vertical shifting procedure is required for the loss modulus.

slightly less than the smallest slope of the curves in Figure 3. This results in a decrease in the instantaneous elastic modulus of about 0.5 GPa as the temperature increases from  $-100^\circ\text{C}$  to  $25^\circ\text{C}$ .

The resulting master curves and shift factors are shown in Figures 7 and 8. Observe that the optimal horizontal shifts for the storage and loss moduli are now nearly identical except at the highest temperatures. The smooth master curves in Figure 7 were generated from the same shift factors, which are essentially the average of those in Figure 8. The coefficients  $G_\infty$  and  $G_n$  in (3) were then fit to this storage modulus master curve using 35 terms. When used in the Prony series (1), these yield a smooth master curve for the stress relaxation function  $G(t, T_0)$  that covers 20 decades of time. A portion of that curve, corrected for room temperature using the appropriate shift factor from Figure 8, is shown in Figure 9.

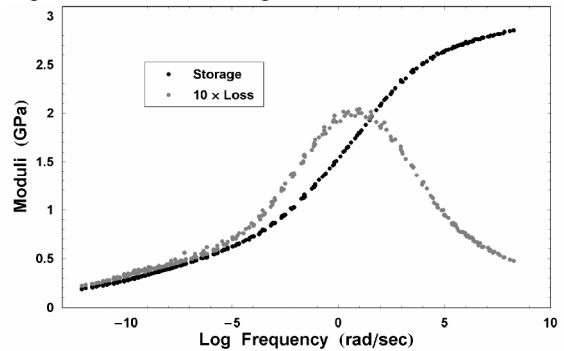


**FIGURE 7. Storage and loss moduli master curves with vertical shifts, using the same optimal averaged horizontal shifts.**

Also shown in figure 7 is an 8-term fit for the time window spanning 0.25 ns to 30 ms. This should be more than sufficient for most impact simulations.

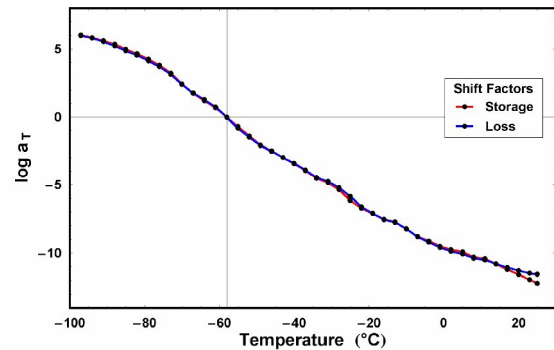


**FIGURE 8. Optimal horizontal shift factors for the storage and loss moduli after vertical shifts.**

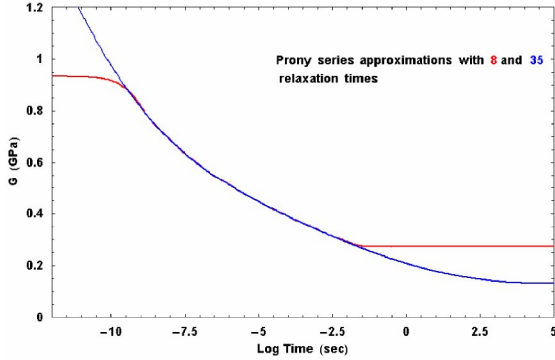


**FIGURE 9. Prony series approximations to the stress relaxation function at 23°C.**

### Damage Parameters

As stated earlier, the total strain rate is the sum of the deviatoric viscoelastic strain rate and the deviatoric cracking strain rate. This generalization allows ductile or brittle material behavior in the fracture model. The failure model assumes that for each element a penny-shaped micro-crack exists normal to the direction of the maximum (principal) deformation rate, as shown in Figure 10.

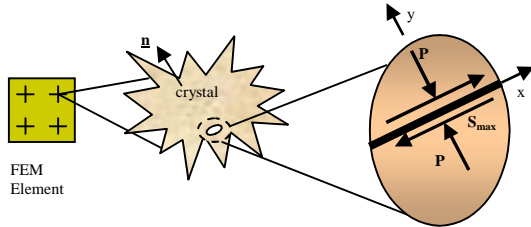


**FIGURE 10. The viscoSCRAM hot spot model showing friction generated along a crack face<sup>9</sup>.**

The deviatoric cracking strain rate is derived as a function of the average crack radius,  $c$ , and the initial flaw size,  $a$ . An evolution equation for the crack growth rate is assumed to depend on the stress intensity factor as shown in Figure 11<sup>9</sup>.

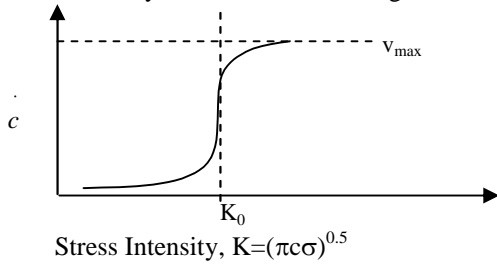


**FIGURE 11. Schematic of crack growth rate,  $c$ .**

A rate-dependent damage function,  $v_{max}$ , is used to calibrate the accumulation of internal damage and appears to be the most important parameter in the damage model. The threshold for stress intensity,  $K_0$ , is a function of the coefficient of static friction,  $\mu_{st}$ , and a stress intensity parameter,  $m$ .  $K_0$  is also related to the effective deviatoric strain rate (at each time increment) in order to convert from a tensor form to an equivalent unidirectional strain rate. This is why the current version of viscoSCRAM is isotropic. The values for  $K_0$ ,  $m$ , and  $\mu_{st}$  are varied from material to material. Since  $v_{max}$  controls the yield strength of the material, it is necessary to optimize  $v_{max}$  to at least three different compressive or tensile loading rates.

### Hot Spot Ignition Model

Thermal heating in viscoSCRAM includes bulk heating at the continuum length scale and hot spot heating at the microstructural length scale. Bulk heating includes mechanical terms describing viscous, damage, and adiabatic volume change as well as, a chemical decomposition term. Chemical decomposition is based on Arrhenius first order chemical kinetics. For the continuum, the rate of temperature change with respect to time is written

$$\dot{T} = -\gamma T \dot{\epsilon}_{kk} + \frac{\mathfrak{F}}{\rho c_v} \left[ (\dot{W})_{ve} + (\dot{W})_{cr} \right] + P_{he} \dot{q}_{ch} \quad (12)$$

where the first term on the right hand side represents adiabatic compression heating rate, the second term represents the inelastic work rates due to viscoelastic effects and cracking damage, and the third term is the bulk chemical heating rate.

The ignition criterion in the viscoSCRAM hot spot model describes frictional heating due to crack faces sliding. Given the stresses from two adjacent elements, the local strain energy release rate is determined. Then, at the end of a time step in the simulation, the change in crack length of the interface crack is determined. If the interface crack grows to be wider than the length of the element edge, the interface fails and is allowed to separate by not enforcing the constraints on the adjacent interface nodes. As the simulation progresses, the failed interfaces coalesce into macroscopic cracks. Once the shear stress exceeds a slip criterion, the adjacent crack faces are assumed to slip. The work done by the slipping faces will generate heat and possibly ignite the energetic. This frictionally

triggered hot spot model is included in the energy balance on a differential material volume near the crack face along with mechanical and chemical heating terms (contribution of heat conduction can be neglected). Referring to Figure 10, the heat transfer near the 1-D crack face is given by

$$\rho_f c_f \dot{T} = k_f T_{,ii} + \rho_f \Delta H Z e^{-\frac{E}{RT}} + \mu_{st} p \dot{\epsilon}_{ij}, \quad l_f \geq y \geq 0 \quad (13)$$

$$\rho_s c_s \dot{T} = k_s T_{,ii} + \rho_s \Delta H Z e^{-\frac{E}{RT}}, \quad y > l_f \quad (14)$$

where the hot spot length scale is  $l_f$  and  $\mu_{st}$  is the coefficient of static friction. In eqns. (13) and (14), the left hand side is the heat stored in the region of the hot spot. The first term on the right side is the heat conducted away from the hot spot and the second term is the chemical heat generation per unit volume. For each finite element, the deviatoric stress is found on a plane normal to the direction of the maximum principal deformation rate. If the maximum shear stress exceeds the value of  $\mu_{st} p$  then the crack is assumed to slip and generate heat. Note that  $p$  is the compressive pressure and if it is positive the crack is open and will not generate heat.

## COMPUTATIONAL RESULTS

The simulations of the shear punch validation test were performed on a parallel computer platform at the ARL MSRC using the LLNL code ALE3D<sup>15</sup>. The entire computational domain included the incident and output bars, the specimen, and the specimen holder. For the simulations presented, the 50cm striker bar was replaced with a prescribed input velocity boundary condition on the end nodes of the incident bar. The z-velocity pulse had a 1300m/s material velocity, a 5 $\mu$ s rise time with duration of 200 $\mu$ s.

A hybrid computational domain was also built for the simulations using 8-node hexagonal elements. Slide surfaces and symmetry conditions were also used to create the 1/4-symmetry, butterfly computational domain, as shown in Figure 12. The input bar, output bar and specimen holder were modeled using an elastic-plastic description. The specimen constitutive behavior was described using the viscoSCRAM model.

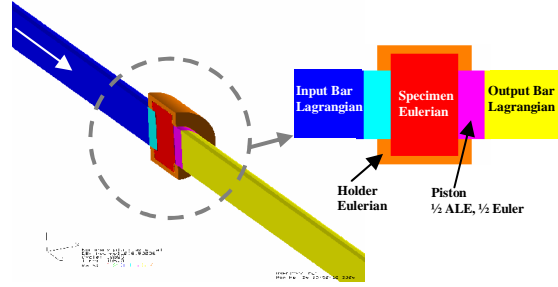


**FIGURE 12. The hybrid computational domain used for the shear punch simulations.**

A plot of the deformed mesh for the specimen is shown in Figure 13. Note the localized shear surface that formed in the specimen. The localized strain in the specimen emanated from the periphery of the indenting piece and, later in time, formed on the distal end at the holder/output bar interface. Figure 13 also shows a plot of the surrogate specimen temperature at the end of the simulation. PC has a melt temperature of 558 K. The temperature rise is due to the conversion of plastic work to heat. Although the temperature localizes near the bar/specimen interface, it dissipates to neighboring elements because of the mesh resolution. For a finer mesh, the temperature may localize along the idealized shear surface and reach a higher order of magnitude.

The specimen geometry is different from what is required in a conventional Kolsky bar. For this reason the strain rate is not uniform in the shear punch specimen. The specimen's strain rate reaches  $\sim 8000-9000s^{-1}$  and localizes along the idealized shear surface. An examination of the shear stress in the specimen during compressive loading at 600 $\mu$ s, shows the stresses reach 40-50 MPa. By comparison the principal compressive stress reaches  $\sim 150$ MPa in the center region and  $\sim 300$ MPa in the outer region. Of course, the state of stress in the specimen will change at the arrival of the transmitted wave. For a finer specimen mesh resolution subjected to this complex state of stress, the specimen material may form adiabatic shear bands. We also note that the pressure in the PC specimen reaches approximately -5MPa (tensile hydrostatic stress). This pressure is above the fracture pressure (-80MPa) therefore, the PC specimen did not fracture in this simulation.

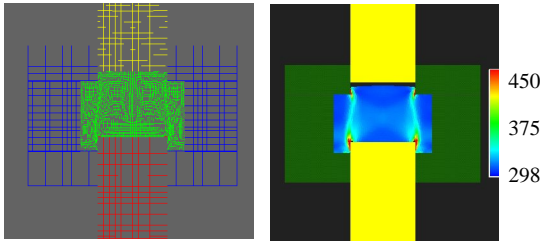


**FIGURE 13. Final deformed shape and temperature [K] in the surrogate PC specimen.**

A comparison of the strain gage signals to the observed result shows excellent agreement, as shown in Figure 14. The incident and reflected pulses are shown in Figure 14a. The curvature at the beginning of the experimental input pulse is due to wave shapers added in front of the input bar. There were no wave shapers added in the numerical simulations. The ringing seen at the beginning and end of the numerical incident signal are due to the sharp discontinuity of the prescribed velocity boundary condition. Smoothing this boundary condition will reduce the ringing.

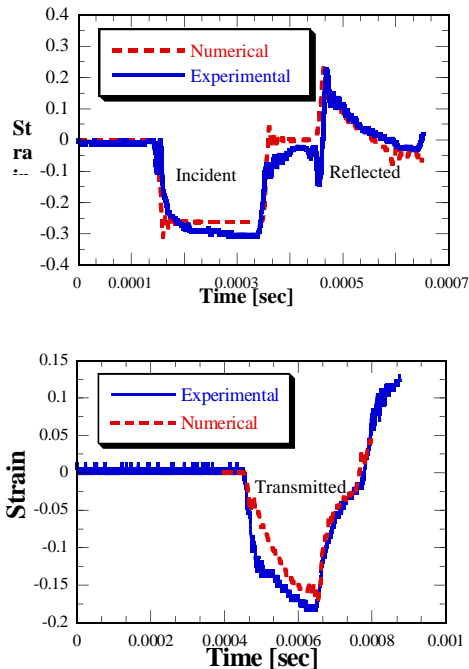


**FIGURE 14. Comparison of strain signals for the incident bar strain gage and the transmitted strain signal.**

The viscoSCRAM constitutive model described was used to represent the behavior of the double-base propellant specimen in the dynamic shear punch test, as shown in Figure 15. New crack faces are created during the early loading stages. As a result, Figure 15 illustrates that the propellant generates heat due to chemical decomposition shortly after the arrival of the dynamic compression wave. In the experiment, the double base propellant experienced more plastic deformation and cracking (resembled an extrusion process) before it generated heat from chemical decomposition.

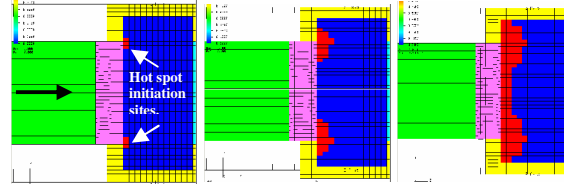


**FIGURE 15. Evolution of chemical heat generation using the viscoSCRAM model.**

## SUMMARY AND CONCLUSIONS

Numerical simulations of a shear punch test have been completed to study the effects of shear loading on various energetics. To date we have completed simulations for nonenergetic polymer materials, plastic bonded explosives, and double base propellants. For viscoelastic parameters, vertical and horizontal shifts of DMA data should be performed to obtain a set of storage and loss modulus master curves. For the damage model, the parameters that control the yield strength must be compared and fitted with observed data to obtain a damage law. Simulations showed excellent agreement of the strain gage signals and showed the general trend of an idealized shear surface in the specimen. The hybrid mesh capability enabled complete modeling of the shear punch test. The Lagrangian formulation used for the incident bar and output bar provided an efficient solution to wave propagation. The ALE mesh for the specimen prevented hourglassing and excessive material advection while maintaining a reasonable timestep. More work is needed to reduce the advection in the specimen for the simulations, i.e. make the specimen more Lagrangian.

The hot spot shear initiation model was included in viscoSCRAM for a double-base propellant. The simulation predicted chemical heat generation at the early stages during the arrival of

the dynamic compression wave. Further work is required on determining the sensitivity of viscoSCRAM input parameters. Furthermore, the authors believe that the isotropic behavior of the damage function causes cracks to accumulate in all directions. Zuo et al.<sup>16</sup> recently showed the importance of stable and unstable orientation on shear cracks. Since the viscoSCRAM model is a “work in progress”, a re-formulation of the damage function into a tensor quantity would directly influence ignition criteria. This would progress viscoSCRAM into a very useful model for predicting insensitive munition behavior.

## REFERENCES

1. Field, J.E., Bourne, N.K., Palmer, S.P., and Walley, S.M., “Hot-Spot Ignition Mechanisms for Explosives and Propellants” *Phil. Trans. of the Roy. Soc. London, A*, Vol. 339, pp.269-283, 1992.
2. Bowden F.P. and Joffe, A.D, *Initiation and Growth of Explosion in Liquids and Solids*. Cambridge University Press, 1952.
3. Davis, W.C., *Los Alamos Sci.*, Vol.2 (1), 1981.
4. Field, J.E., Swallowe, G.M. and Heavens, S.N., “Ignition Mechanisms of Explosives During Mechanical Deformation” *Proc. R. Soc. Lond. A*, Vol. 382, pp. 269-283, 1982.
5. Dienes, J.K., “Frictional Hot-spots and Propellant Sensitivity” *Proc. Mat. Res. Soc. Symp.*, Vol. 24, 1984.
6. Kubota, N. *Propellants and Explosives: Thermochemical Aspects of Combustion*, Wiley-VCH, 2002.
7. Boyle, V., Frey, R., and Blake, O., “Combined Pressure Shear Ignition of Explosives” *Proceedings of the 9<sup>th</sup> International Detonation Symposium*, OCNR 113291-7.
8. Krzewinski, B., Lieb, R., Baker, P., VandeKieft, L., “Shear Deformation and Shear Initiation of Explosives and Propellants” *Proceedings of the 12<sup>th</sup> International Detonation Symposium*, 2002.
9. Bennett, J.G., Haberman, K.S., Johnson, J.J., Asay, B.W., and Henson, B.F., “A Constitutive Model for the Non-Shock Ignition and Mechanical Response of High Explosives” *J. Mech. Phys. Solids*, Vol. 46, pp.2303-2322, 1998.
10. Addesio, F.L. and Johnson, J.N., “A Constitutive Model for the Dynamic Response of Brittle Materials” *Journal of Appl. Phys.*, Vol. 67, pp. 3275-3286, 1990.
11. Dienes, J.K., “A Unified Theory of Flow, Hot-spots, and Fragmentation with an Application to Explosive Sensitivity” in *High Pressure Shock Compression of Solids II: Dynamic Fracture and Fragmentation*, L. Davidson et al., eds., Springer, New York, pp.366-398.
12. Simon, P. P., and Ploehn, H. J., “Investigating Time-Temperature Superpositioning in Crosslinked Polymers Using the Tube Junction Model” *J. Polymer Sci.*, Vol. 37, pp. 127-142, 1999.
13. McCrum, N. G., and Pogany, G. A., “Time-Temperature Superposition in the  $\alpha$  Region of an Epoxy Resin” *J. Macromol. Sci. – Phys.*, Vol. B4(1), pp. 109-126, 1970.
14. Schapery, R. A., “Viscoelastic Behavior and Analysis of Composite Materials”, in *Composite Materials Vol. 2: Mechanics of Composite Materials*, edited by G. P. Sendeckyj, pp. 85-168, Academic press, New York, 1974.
15. Sharp, R., and the ALE3D Team, “Users Manual for ALE3D v.3.8.5” *Lawrence Livermore National Laboratories UCRL-MA-152204*, 2004.
16. Zou, Q.H., Addesio, F.L., Dienes, J.K., and Lewis, M.W., “A Rate-Dependant Damage Model for Brittle Materials Based on the Dominant Crack” *Int. J. of Solids and Structures*, Vol. 43, pp. 3350-3380, 2006.

NO. OF  
COPIES ORGANIZATION

1 DEFENSE TECHNICAL  
(PDF INFORMATION CTR  
only) DTIC OCA  
8725 JOHN J KINGMAN RD  
STE 0944  
FORT BELVOIR VA 22060-6218

1 DIRECTOR  
US ARMY RESEARCH LAB  
IMNE ALC HRR  
2800 POWDER MILL RD  
ADELPHI MD 20783-1197

1 DIRECTOR  
US ARMY RESEARCH LAB  
RDRL CIM L  
2800 POWDER MILL RD  
ADELPHI MD 20783-1197

1 DIRECTOR  
US ARMY RESEARCH LAB  
RDRL CIM P  
2800 POWDER MILL RD  
ADELPHI MD 20783-1197

ABERDEEN PROVING GROUND

1 DIR USARL  
RDRL CIM G (BLDG 4600)

NO. OF  
COPIES ORGANIZATION

ABERDEEN PROVING GROUND

22 DIR USARL  
RDRL WMM D  
B CHEESEMAN  
C-F YEN  
RDRL WMT  
P BAKER  
RDRL WMT A  
J RUNYEON  
S SCHOENFELD  
RDRL WMT B  
N ELDREDGE  
R GUPTA  
S KUKUCK  
R BANTON  
RDRL WMT C  
T BJERKE  
S SCHRAML  
RDRL WMT D  
N GNIAZDOWSKI  
S BILYK (5 CPS)  
E RAPACKI  
R KRAFT  
M GREENFIELD  
B LOVE  
RDRL WMT E  
B RINGERS